Finite Element Approach for Radiative Transfer in Multi-Layer Graded Index Cylindrical Medium with Fresnel Surfaces

L. Zhang, J.M. Zhao, L.H. Liu*

School of Energy Science and Engineering, Harbin Institute of Technology, 92 West Dazhi Street, Harbin 150001, People's Republic of China

ABSTRACT

Because the optical plane defined by the incidence and reflection direction at a cylindrical surface has a complicated relation with the local azimuthal angle and zenith angle in the traditional cylindrical coordinate system, it is difficult to deal with the specular reflective boundary condition in the solution of the traditional radiative transfer equation for cylindrical system. In this paper, a **N**ew **R**adiative **T**ransfer **E**quation for **G**raded index medium in **C**ylindrical system (RTEGCN) is derived based on a new defined cylindrical coordinate system. In this new cylindrical coordinate system, the optical plane defined by the incidence and reflection direction is just the isometric plane of the local azimuthal angle, which facilitates the RTEGCN in dealing with cylindrical specular reflective boundaries. A least squares finite element method (LSFEM) is developed for solving radiative transfer in single and multi-layer cylindrical medium based on the discrete ordinates form of the RTEGCN. For multi-layer cylindrical medium, a radial basis function interpolation method is proposed to couple the radiative intensity at the interface between two adjacent layers. Various radiative transfer problems in both single and multi-layer cylindrical medium are tested. The results show that the present finite element approach has good accuracy to predict the radiative heat transfer in multi-layer cylindrical medium with Fresnel surfaces.

Keywords: Finite element method; radiative transfer; multi-layer medium; Fresnel boundary; graded index

---

*Tel.: +86-451-86402237; fax: +86-451-86221048.

Email address: lhliu@hit.edu.cn

NOMANCLATURE

$\mathbf{e}_\rho$, $\mathbf{e}_\Psi$, $\mathbf{e}_z$	Unit vectors of the ρ-, Ψ- and z-directions, respectively
$\mathbf{H}$	Matrix defined in Eq. (29b)
I	Radiative intensity
I_b	Blackbody radiative intensity
$I_{i,L}(\theta)$, $I_{i,R}(\theta)$	The radiative intensity of left and right side of *i*th interface
$\mathbf{n}$	Unit normal vector
n	Refractive index
N_{sol}	Total number of solution nodes
q_ρ	Radiative heat flux of radial direction, W/m^2
$\mathbf{r}$	Vector of spatial position
R	Radius of cylindrical medium, m
R_i, R_o	Radius of inner and outer layer, m
R_S, R_P	Reflectivity of S polarization and P polarization
$\tilde{S}$	Variable defined in Eq. (26b)
T	Temperature, K
T_0	Surrounding temperature, K
T_g	Medium temperature, K
V	Solution domain
W	Weight function

Greek Symbols

α_V	Dimensionless volumetric absorption

$\boldsymbol{\alpha}$	Vector defined in Eq. (36)
$\tilde{\beta}$	Variable defined in Eq. (26a)
χ_θ, χ_φ	Difference coefficients defined by Eq. (24)
ε_w	Wall emissivity
ϕ	Finite element shape function
Φ	Scattering phase function
$\boldsymbol{\Phi}$	Matrix defined in Eq. (36)
φ	Azimuthal angle
$\Delta\varphi$	Azimuthal angle step
κ_a	Absorption coefficient, m^{-1}
κ_s	Scattering coefficient, m^{-1}
$\mu^{m,n}, \xi^{m,n}, \eta^{m,n}$	Direction cosine of the direction (m,n)
θ	Polar angle
$\tilde{\theta}$, θ''	Refraction and reflection directions of polar angle θ, respectively
$\Delta\theta$	Polar angle step
ρ_f	Fresnel reflection coefficient
ρ, Ψ, z	Cylindrical coordinates defined in solution domain
σ	Stefan-Boltzmann constant, W/m^2K^4
τ_R	Optical thickness, $\tau_R = (\kappa_a + \kappa_s) R$
ω	Single scattering albedo, $\omega = \kappa_s / (\kappa_a + \kappa_s)$
$\boldsymbol{\Omega}, \boldsymbol{\Omega}'$	Vector of radiation direction, $\boldsymbol{\Omega} = \mu \mathbf{e}_\rho + \eta \mathbf{e}_\Psi + \xi \mathbf{e}_z$
Ω	Solid angle
$\Re$	Radial basis function

Subscripts

i, j	Solution node index
w	Value at wall boundary

Superscripts

$m, m', n, n', m \pm 1/2, n \pm 1/2$	Angular indices

1 INTRODUCTION

Numerical analysis of radiative transfer in participating media plays an important role in engineering applications. Due to the structural characteristics of material or temperature and/or concentration dependency, the refractive index of a medium will show some spatially varied distribution, which violates the assumption of uniform distribution of refractive index in traditional radiative transfer analysis. Recently, radiative transfer in variable refractive index or graded index medium has attracted the interest of many researchers [1-5].

As is well known, the most effective way to deal with cylindrical geometries is in cylindrical coordinates, though the methods formulated in Cartesian coordinates are capable of solving radiative transfer in such geometries. As for radiative transfer in semitransparent graded index cylindrical medium, Ben Abdallah et. al [6] derived an integral form of radiative transfer equation inside refractive cylindrical media and solved the temperature distribution inside fibers. The ray tracing method used in Ref. [6] is computational complex and difficult. Recently, Liu et al. [7] derived the **R**adiative **T**ransfer **E**quation for **G**raded index medium in the traditional **C**ylindrical coordinate system [8] (RTEGC) as shown in Fig. 1(a), which is a basis to develop efficient differential approach to solve radiative transfer in graded index cylindrical medium. Based on the RTEGC [7], Zhang et. al [9] developed an efficient finite element approach for radiative transfer in multi-dimensional graded

index cylindrical medium with diffuse boundaries.

It often happens that the interface of medium and surroundings is Fresnel surface, such as the radiative transfers in organism and optical fiber. Due to the Fresnel effects, there are additional modeling difficulties which arise from the dramatic change of reflectivity near the critical angle. Fresnel boundary is often supposed as diffuse boundary [10, 11], which generally introduces computational errors. However, it is found to be inconvenient to deal with the specular reflective boundary condition in the traditional cylindrical coordinate system [Fig. 1(a)], which is due to the optical plane defined by incident and reflection direction at a cylindrical surface has a complicate relation with the local azimuthal angle φ' and zenith angle θ', and the incident direction and reflected direction at the cylindrical boundary are not easily to be related in the local angular coordinates.

In this paper, a **N**ew **R**adiative **T**ransfer **E**quation formulated for **G**raded index medium in **C**ylindrical system (RTEGCN) is derived based on a new defined cylindrical coordinate system, with which the Fresnel boundary condition can be easily handled. A least squares finite element method (LSFEM) is then developed for solving radiative transfer in cylindrical medium with Fresnel surfaces based on the discrete ordinates form of the RTEGCN. The method is enhanced to solve radiative transfer in multi-layer cylindrical medium with the help of a radial basis function interpolation method to couple the radiative intensity at the interface between two adjacent layers. Finally, four various test problems of both solid cylinder and multilayer cylinder, and with medium of uniform refractive index distribution and graded refractive index distribution are taken to verify the finite element formulation.

2 MATHEMATICAL FORMULATION

2.1 A New Radiative Transfer Equation for Graded Index Medium in Cylindrical Coordinate System

The main difference between the new defined cylindrical coordinate system and the traditional one lies in the definition of local angular coordinates. The definition of the new cylindrical coordinate system is shown in Fig.1

(b), in which the local zenith angle θ is defined based on the local radial direction $\mathbf{e}_\rho$. Because $\mathbf{e}_\rho$ also serves as the normal vector of the cylindrical boundary, according to Snell's law, the optical plane defined by the incidence and reflection direction is just the isometric plane of the local azimuthal angle φ in this new cylindrical coordinate system. In the optical plane, the local zenith angle of the reflection direction θ_i' holds a simple relationship with incidence direction θ_i as $\theta_i + \theta_i' = \pi$, which is the same as the case of one dimensional slab, thus facilitates the treatment of Fresnel reflection and refraction at cylindrical boundary. In the following, the radiative transfer equation for graded index medium in this new cylindrical coordinate system is derived. The radiative transfer equation for graded index medium along the ray trajectory s can be written as

$$n^2 \frac{\mathrm{d}}{\mathrm{d}s}\left[\frac{I(\mathbf{r},\mathbf{\Omega})}{n^2}\right] = -\left(\kappa_a + \kappa_s\right) I(\mathbf{r},\mathbf{\Omega}) + n^2 \kappa_a I_b(\mathbf{r}) + \frac{\kappa_s}{4\pi}\int_{4\pi} I(\mathbf{r},\mathbf{\Omega})\Phi(\mathbf{\Omega}',\mathbf{\Omega})\,\mathrm{d}\Omega' \tag{1}$$

where $\mathrm{d}/\mathrm{d}s$ is the streaming operator; $I(\mathbf{r},\mathbf{\Omega})$ is the radiative intensity, which is a function of spatial position $\mathbf{r}$ and direction $\mathbf{\Omega}$; $I_b(\mathbf{r})$ is the blackbody radiative intensity at the temperature of the medium; n is the refractive index of medium, which is a function of spatial position; κ_a and κ_s are the absorption and the scattering coefficients, respectively; $\Phi(\mathbf{\Omega}',\mathbf{\Omega})$ is the scattering phase function indicating scattering from the incoming direction $\mathbf{\Omega}'$ to the outgoing direction $\mathbf{\Omega}$.

The major task to express Eq. (1) in the new cylindrical coordinate system [Fig.1 (b)] is to expand the streaming operator $\mathrm{d}/\mathrm{d}s$ in this coordinate system. Similar to the traditional cylindrical coordinate system, the radiative intensity in the new cylindrical coordinate system is also a function of spatial position and angular coordinates. Following the ray trajectory, the streaming operator $\mathrm{d}/\mathrm{d}s$ can be expanded as [12]

$$\frac{\mathrm{d}}{\mathrm{d}s} = \frac{\mathrm{d}\rho}{\mathrm{d}s}\frac{\partial}{\partial\rho} + \frac{\mathrm{d}\psi}{\mathrm{d}s}\frac{\partial}{\partial\psi} + \frac{\mathrm{d}z}{\mathrm{d}s}\frac{\partial}{\partial z} + \frac{\mathrm{d}\theta}{\mathrm{d}s}\frac{\partial}{\partial\theta} + \frac{\mathrm{d}\varphi}{\mathrm{d}s}\frac{\partial}{\partial\varphi} \tag{2}$$

As seen from Eq. (2), five differential coefficients are needed to expand the streaming operator. The first three differential coefficients, namely $\frac{\mathrm{d}\rho}{\mathrm{d}s}$, $\frac{\mathrm{d}\psi}{\mathrm{d}s}$ and $\frac{\mathrm{d}z}{\mathrm{d}s}$ are related to spatial coordinates, while the last two $\frac{\mathrm{d}\theta}{\mathrm{d}s}$ and $\frac{\mathrm{d}\varphi}{\mathrm{d}s}$ are related to local angular coordinates. These differential coefficients will be derived in the following.

The definition of the cylindrical coordinates in Fig. 1(b) yields

$$\mathrm{d}\rho = \cos\theta\,\mathrm{d}s\,,\quad \rho\,\mathrm{d}\psi = \sin\theta\cos\varphi\,\mathrm{d}s\,,\quad \mathrm{d}z = \sin\theta\sin\varphi\,\mathrm{d}s \tag{3}$$

which give the spatial differential coefficients, and Eq. (2) is further written as

$$\frac{\mathrm{d}}{\mathrm{d}s} = \mathbf{\Omega}\bullet\nabla + \frac{\mathrm{d}\theta}{\mathrm{d}s}\frac{\partial}{\partial\theta} + \frac{\mathrm{d}\varphi}{\mathrm{d}s}\frac{\partial}{\partial\varphi} \tag{4}$$

where $\mathbf{\Omega} = \mu\mathbf{e}_\psi + \eta\mathbf{e}_z + \xi\mathbf{e}_\rho$ is the local direction vector of the beam; $\mu = \sin\theta\cos\varphi$, $\eta = \sin\theta\sin\varphi$ and $\xi = \cos\theta$, which are the direction cosines of the beam direction. The gradient operator ∇ in this cylindrical coordinates is

$$\nabla = \frac{1}{\rho}\frac{\partial}{\partial\psi}\mathbf{e}_\psi + \frac{\partial}{\partial\mathrm{z}}\mathbf{e}_z + \frac{\partial}{\partial\rho}\mathbf{e}_\rho \tag{5}$$

From the definition of direction cosines, it follows that

$$\frac{\mathrm{d}\mu}{\mathrm{d}s} = \cos\theta\cos\varphi\frac{\mathrm{d}\theta}{\mathrm{d}s} - \sin\theta\sin\varphi\frac{\mathrm{d}\varphi}{\mathrm{d}s} \tag{6a}$$

$$\frac{\mathrm{d}\eta}{\mathrm{d}s} = \cos\theta\sin\varphi\frac{\mathrm{d}\theta}{\mathrm{d}s} + \sin\theta\cos\varphi\frac{\mathrm{d}\varphi}{\mathrm{d}s} \tag{6b}$$

$$\frac{\mathrm{d}\xi}{\mathrm{d}s} = -\sin\theta\frac{\mathrm{d}\theta}{\mathrm{d}s} \tag{6c}$$

and hence the angular differential coefficients $\frac{\mathrm{d}\theta}{\mathrm{d}s}$ and $\frac{\mathrm{d}\varphi}{\mathrm{d}s}$ can be expressed as

$$\frac{\mathrm{d}\varphi}{\mathrm{d}s} = \frac{1}{\sin\theta}\left(\cos\varphi\frac{\mathrm{d}\eta}{\mathrm{d}s} - \sin\varphi\frac{\mathrm{d}\mu}{\mathrm{d}s}\right) \tag{7a}$$

$$\frac{\mathrm{d}\theta}{\mathrm{d}s} = -\frac{1}{\sin\theta}\frac{\mathrm{d}\xi}{\mathrm{d}s} \tag{7b}$$

where $\frac{\mathrm{d}\mu}{\mathrm{d}s}$, $\frac{\mathrm{d}\eta}{\mathrm{d}s}$ and $\frac{\mathrm{d}\xi}{\mathrm{d}s}$ are unknown and needed to be derived from the ray equation [7]. By definition, the local direction vector $\mathbf{\Omega}$ can be obtained from the spatial vector $\mathbf{r} = \rho\cos\psi\,\mathbf{i} + \rho\sin\psi\,\mathbf{j} + z\,\mathbf{k}$ in the cylindrical coordinates as

$$\begin{aligned}\mathbf{\Omega} &= \mu\mathbf{e}_\psi + \eta\mathbf{e}_z + \xi\mathbf{e}_\rho \\ &= \frac{\mathrm{d}\mathbf{r}}{\mathrm{d}s} = \mu(\cos\psi\,\mathbf{j} - \sin\psi\,\mathbf{i}) + \eta\,\mathbf{k} + \xi(\cos\psi\,\mathbf{i} + \sin\psi\,\mathbf{j})\end{aligned} \tag{8}$$

From the ray equation $\frac{\mathrm{d}}{\mathrm{d}s}\left(n\frac{\mathrm{d}\mathbf{r}}{\mathrm{d}s}\right) = \nabla n$, namely, $\frac{\mathrm{d}}{\mathrm{d}s}\left(n\,\mathbf{\Omega}\right) = \nabla n$, it follows that

$$\frac{\mathrm{d}\mathbf{\Omega}}{\mathrm{d}s}=\frac{\nabla n}{n}-\mathbf{\Omega}\frac{1}{n}\frac{\mathrm{d}n}{\mathrm{d}s}=\frac{\nabla n}{n}-\mathbf{\Omega}\frac{\mathbf{\Omega}\bullet\nabla n}{n} \tag{9}$$

At the same time

$$\frac{\mathrm{d}\mathbf{\Omega}}{\mathrm{d}s}=\mu\frac{\mathrm{d}\mathbf{e}_{\psi}}{\mathrm{d}s}+\eta\frac{\mathrm{d}\mathbf{e}_{z}}{\mathrm{d}s}+\xi\frac{\mathrm{d}\mathbf{e}_{\rho}}{\mathrm{d}s}+\frac{\mathrm{d}\mu}{\mathrm{d}s}\mathbf{e}_{\psi}+\frac{\mathrm{d}\eta}{\mathrm{d}s}\mathbf{e}_{z}+\frac{\mathrm{d}\xi}{\mathrm{d}s}\mathbf{e}_{\rho} \tag{10}$$

Using Eq. (8) and the relations given in Eq. (3), it yields

$$\frac{\mathrm{d}\mathbf{e}_{\psi}}{\mathrm{d}s}=-\frac{\mu}{\rho}\mathbf{e}_{\rho},\ \ \frac{\mathrm{d}\mathbf{e}_{z}}{\mathrm{d}s}=\mathbf{0},\ \ \frac{\mathrm{d}\mathbf{e}_{\rho}}{\mathrm{d}s}=\frac{\mu}{\rho}\mathbf{e}_{\psi} \tag{11}$$

hence

$$\frac{\mathrm{d}\mathbf{\Omega}}{\mathrm{d}s}=-\frac{\mu^{2}}{\rho}\mathbf{e}_{\rho}+\xi\frac{\mu}{\rho}\mathbf{e}_{\psi}+\frac{\mathrm{d}\mu}{\mathrm{d}s}\mathbf{e}_{\psi}+\frac{\mathrm{d}\eta}{\mathrm{d}s}\mathbf{e}_{z}+\frac{\mathrm{d}\xi}{\mathrm{d}s}\mathbf{e}_{\rho} \tag{12}$$

By dot product equation (9) with $\mathbf{e}_{\psi}$, $\mathbf{e}_{\rho}$ and $\mathbf{e}_{z}$, and combine Eq. (9), it follows that

$$\frac{\mathrm{d}\mu}{\mathrm{d}s}=\frac{1}{n}\frac{\partial n}{\rho\partial\psi}-\mu\frac{\mathbf{\Omega}\bullet\nabla n}{n}-\xi\frac{\mu}{\rho} \tag{13a}$$

$$\frac{\mathrm{d}\eta}{\mathrm{d}s}=\frac{1}{n}\frac{\partial n}{\partial z}-\eta\frac{\mathbf{\Omega}\bullet\nabla n}{n} \tag{13b}$$

$$\frac{\mathrm{d}\xi}{\mathrm{d}s}=\frac{1}{n}\frac{\partial n}{\partial\rho}-\xi\frac{\mathbf{\Omega}\bullet\nabla n}{n}+\frac{\mu^{2}}{\rho} \tag{13c}$$

Substitute Eq. (13) into Eq. (7), the angular differential coefficients are obtained as

$$\frac{\mathrm{d}\varphi}{\mathrm{d}s}=\frac{1}{\sin\theta}\left(\cos\varphi\frac{1}{n}\frac{\partial n}{\partial z}-\sin\varphi\frac{1}{n}\frac{\partial n}{\rho\partial\psi}\right)+\xi\frac{\sin\varphi\cos\varphi}{\rho} \tag{14a}$$

$$\frac{\mathrm{d}\theta}{\mathrm{d}s}=-\frac{1}{\sin\theta}\left[\frac{1}{n}\frac{\partial n}{\partial\rho}-\xi\frac{\mathbf{\Omega}\bullet\nabla n}{n}+\frac{\mu^{2}}{\rho}\right] \tag{14b}$$

Therefore, the streaming operator $\mathrm{d}/\mathrm{d}s$ in Eq. (4) can be written as

$$\begin{aligned}\frac{\mathrm{d}}{\mathrm{d}s}=&\mathbf{\Omega}\bullet\nabla+\xi\frac{\sin\varphi\cos\varphi}{\rho}\frac{\partial}{\partial\varphi}-\mu\frac{\cos\varphi}{\rho}\frac{\partial}{\partial\theta}\\&+\frac{1}{\sin\theta}\left[\mathbf{s}_{1}\bullet\frac{\nabla n}{n}\right]\frac{\partial}{\partial\varphi}+\frac{1}{\sin\theta}\left[\left(\xi\mathbf{\Omega}-\mathbf{e}_{\rho}\right)\bullet\frac{\nabla n}{n}\right]\frac{\partial}{\partial\theta}\end{aligned} \tag{15}$$

where the vector $\mathbf{s}_{1}$ is defined as $\mathbf{s}_{1}=-\sin\varphi\mathbf{e}_{\psi}+\cos\varphi\mathbf{e}_{z}+0\mathbf{e}_{\rho}$. By using the following relation,

$$n^2 \frac{\mathrm{d}}{\mathrm{d}s}\left[\frac{f}{n^2}\right] = \frac{\mathrm{d}f}{\mathrm{d}s} - 2f\frac{1}{n}\frac{\mathrm{d}n}{\mathrm{d}s} = \frac{\mathrm{d}f}{\mathrm{d}s} - 2\frac{\mathbf{\Omega}\bullet\nabla n}{n} f \tag{16}$$

the radiative transfer equation for graded index medium in the new cylindrical coordinate system (RTEGCN) can be expressed in a non-conservative form as

$$\begin{aligned}
&\mathbf{\Omega}\bullet\nabla I(\mathbf{r},\mathbf{\Omega}) + \xi\frac{\sin\varphi\cos\varphi}{\rho}\frac{\partial}{\partial\varphi} I(\mathbf{r},\mathbf{\Omega}) - \mu\frac{\cos\varphi}{\rho}\frac{\partial}{\partial\theta} I(\mathbf{r},\mathbf{\Omega}) \\
&+\frac{1}{\sin\theta}\left[\mathbf{s}_1\bullet\frac{\nabla n}{n}\right]\frac{\partial}{\partial\varphi} I(\mathbf{r},\mathbf{\Omega}) + \frac{1}{\sin\theta}\left[\left(\xi\mathbf{\Omega}-\mathbf{e}_\rho\right)\bullet\frac{\nabla n}{n}\right]\frac{\partial}{\partial\theta} I(\mathbf{r},\mathbf{\Omega}) \\
&+\left(\kappa_a+\kappa_s - 2\mathbf{\Omega}\bullet\frac{\nabla n}{n}\right) I(\mathbf{r},\mathbf{\Omega}) = n^2\kappa_a I_b(\mathbf{r}) + \frac{\kappa_s}{4\pi}\int_{4\pi} I(\mathbf{r},\mathbf{\Omega}')\Phi(\Omega',\Omega)\,\mathrm{d}\Omega'
\end{aligned} \tag{17}$$

By setting the gradient of refractive index ∇n to zero, Eq. (17) reduces to

$$\begin{aligned}
&\mathbf{\Omega}\bullet\nabla I(\mathbf{r},\mathbf{\Omega}) + \xi\frac{\sin\varphi\cos\varphi}{\rho}\frac{\partial}{\partial\varphi} I(\mathbf{r},\mathbf{\Omega}) - \mu\frac{\cos\varphi}{\rho}\frac{\partial}{\partial\theta} I(\mathbf{r},\mathbf{\Omega}) \\
&+\left(\kappa_a+\kappa_s\right) I(\mathbf{r},\mathbf{\Omega}) = n^2\kappa_a I_b(\mathbf{r}) + \frac{\kappa_s}{4\pi}\int_{4\pi} I(\mathbf{r},\mathbf{\Omega}')\Phi(\Omega',\Omega)\,\mathrm{d}\Omega'
\end{aligned} \tag{18}$$

which is the radiative transfer equation for uniform index medium in the new cylindrical coordinate system. As compared to the radiative transfer equation in traditional coordinate system , a new angular redistribution term related to zenith angle θ appears, namely the 3rd term in Eq. (18). Following the approach in Ref. [7], a conservative form of the RTEGCN can be derived as

$$\begin{aligned}
&\mu\frac{\partial I(\mathbf{r},\mathbf{\Omega})}{\rho\partial\psi} + \eta\frac{\partial I(\mathbf{r},\mathbf{\Omega})}{\partial \mathrm{z}} + \xi\frac{\partial\rho I(\mathbf{r},\mathbf{\Omega})}{\rho\partial\rho} \\
&+\frac{\partial}{\rho\partial\varphi}\left\{\left[\cos\theta\sin\varphi\cos\varphi\right] I(\mathbf{r},\mathbf{\Omega})\right\} - \frac{1}{\sin\theta}\frac{\partial}{\rho\partial\theta}\left\{\left[\sin^2\theta\cos^2\varphi\right] I(\mathbf{r},\mathbf{\Omega})\right\} \\
&+\frac{1}{\sin\theta}\frac{\partial}{\partial\varphi}\left\{\left[\mathbf{s}_1\bullet\frac{\nabla n}{n}\right] I(\mathbf{r},\mathbf{\Omega})\right\} \\
&+\frac{1}{\sin\theta}\frac{\partial}{\partial\theta}\left\{\left[\left(\xi\mathbf{\Omega}-\mathbf{e}_\rho\right)\bullet\frac{\nabla n}{n}\right] I(\mathbf{r},\mathbf{\Omega})\right\} \\
&+\left(\kappa_a+\kappa_s\right) I(\mathbf{r},\mathbf{\Omega}) \\
&= n^2\kappa_a I_b(\mathbf{r}) + \frac{\kappa_s}{4\pi}\int_{4\pi} I(\mathbf{r},\mathbf{\Omega}')\Phi(\Omega',\Omega)\,\mathrm{d}\Omega'
\end{aligned} \tag{19}$$

Equation (19) contains four angular redistribution terms [the 3rd to 6th term in Eq. (19)]. The 3rd and the 4th terms originate from the connection of the definition of angular coordinates with spatial coordinates. The other two

originate from the graded index of refraction and account for the effect of curved ray trajectory. It is noted that the term $1/\rho$ in Eq.(19) will lead to numerical singularity at the origin where $\rho = 0$. To avoid the numerical singularity at origin $\rho = 0$, a simple approach is to multiply Eq. (19) by ρ, as such the RTEGCN is written as

$$\begin{aligned}
&\mu\frac{\partial I(\mathbf{r},\mathbf{\Omega})}{\partial \psi}+\eta\frac{\rho\partial I(\mathbf{r},\mathbf{\Omega})}{\partial \mathrm{z}}+\xi\frac{\partial \rho I(\mathbf{r},\mathbf{\Omega})}{\partial \rho}\\
&+\frac{1}{\sin\theta}\frac{\partial}{\partial\varphi}\left[\left(\sin\theta\cos\theta\sin\varphi\cos\varphi+\mathbf{s}_1\bullet\frac{\rho\nabla n}{n}\right)I(\mathbf{r},\mathbf{\Omega})\right]\\
&+\frac{1}{\sin\theta}\frac{\partial}{\partial\theta}\left\{\left[\left(\xi\mathbf{\Omega}-\mathbf{e}_\rho\right)\bullet\frac{\rho\nabla n}{n}-\sin^2\theta\cos^2\varphi\right]I(\mathbf{r},\mathbf{\Omega})\right\}\\
&+\rho\left(\kappa_a+\kappa_s\right)I(\mathbf{r},\mathbf{\Omega})=\rho n^2\kappa_a I_b(\mathbf{r})+\rho\frac{\kappa_s}{4\pi}\int_{4\pi}I(\mathbf{r},\mathbf{\Omega}')\Phi(\Omega',\Omega)\,\mathrm{d}\,\Omega'
\end{aligned}\tag{20}$$

In this circumstance, special treatment and additional mathematical boundary conditions are needed in numerical discretization as discussed in [9]. The physical Fresnel boundary condition can be expressed as

$$I(\mathbf{r}_w,\mathbf{\Omega})=\varepsilon_w(\mathbf{\Omega})n^2(\mathbf{r}_w)I_b(\mathbf{r}_w)+\left[1-\varepsilon_w(\mathbf{\Omega})\right]I(\mathbf{r}_w,\mathbf{\Omega}''),\ \ \xi<0 \tag{21}$$

where $\mathbf{\Omega}''$ is the incident direction of specular reflection, $\varepsilon_w(\mathbf{\Omega})$ is the directional emittance defined by Fresnel law, I_b is the blackbody radiative intensity, $\mathbf{n}_w$ is the outward unit normal vector at boundary.

For an infinite long cylinder with axial symmetry, which is the focus of following section of present study, the RTEGCN [Eq.(20)] reduces to

$$\begin{aligned}
&\xi\frac{\partial\rho I(\rho,\mathbf{\Omega})}{\partial\rho}+\frac{\partial}{\partial\varphi}\left\{\left(\cos\theta\sin\varphi\cos\varphi\right)I(\rho,\mathbf{\Omega})\right\}\\
&+\frac{1}{\sin\theta}\frac{\partial}{\partial\theta}\left\{\left[\left(\xi^2-1\right)\frac{\rho}{n}\frac{\partial n}{\partial\rho}-\sin^2\theta\cos^2\varphi\right]I(\rho,\mathbf{\Omega})\right\}\\
&+\rho\left(\kappa_a+\kappa_s\right)I(\rho,\mathbf{\Omega})=\rho n^2\kappa_a I_b(\rho)+\rho\frac{\kappa_s}{4\pi}\int_{4\pi}I(\rho,\mathbf{\Omega}')\Phi(\Omega',\Omega)\,\mathrm{d}\,\Omega'
\end{aligned}\tag{22}$$

2.2 Discrete Ordinates Form of the RTEGCN

Angular discretization is needed before the solution of the RTEGCN. Without loss of generality, only the formulation for an infinite long cylinder with axial symmetry is considered. The discrete ordinates form of the RTEGCN can be derived following a similar procedure presented in Ref. [9] for the derivation of the discrete ordinates form of the RTEGC. The piecewise constant angular approximation (PCA) [13] and step scheme are

taken to discretize these angular redistribution terms. The local zenith and azimuthal angle are discretized as in Ref. [9]. Finite difference discretization of the two angular redistribution terms in Eq. (22) can be written as

$$\left\{\frac{\partial}{\partial\varphi}\left[\cos\theta\sin\varphi\cos\varphi I(\rho,\mathbf{\Omega})\right]\right\}_{\Omega=\Omega^{m,n}} \simeq \frac{\chi_{\varphi}^{m,n+1/2}I^{m,n+1/2}-\chi_{\varphi}^{m,n-1/2}I^{m,n-1/2}}{w_{\varphi}^{n}}, \qquad m=1,...,N_{\theta},\quad n=1,...,N_{\varphi} \tag{23a}$$

$$\left[\frac{1}{\sin\theta}\frac{\partial}{\partial\theta}\left\{\left[\left(\xi^{2}-1\right)\frac{\rho}{n}\frac{\partial n}{\partial\rho}-\sin^{2}\theta\cos^{2}\varphi\right]I(\rho,\mathbf{\Omega})\right\}\right]_{\Omega=\Omega^{m,n}} \simeq \frac{\chi_{\theta}^{m+1/2,n}I^{m+1/2,n}-\chi_{\theta}^{m-1/2,n}I^{m-1/2,n}}{w_{\theta}^{m}}, \qquad m=1,...,N_{\theta},\quad n=1,...,N_{\varphi} \tag{23b}$$

and the recursion formula for $\chi_{\theta}^{m+1/2,n}$ and $\chi_{\varphi}^{m,n+1/2}$ are given as

$$\chi_{\varphi}^{m,n+1/2}-\chi_{\varphi}^{m,n-1/2}=w_{\varphi}^{n}\left\{\frac{\partial}{\partial\varphi}\left[\cos\theta\sin\varphi\cos\varphi\right]\right\}_{\Omega=\Omega^{m,n}} = w_{\varphi}^{n}\cos\theta^{m}\cos 2\varphi^{n} \tag{24a}$$

$$\chi_{\varphi}^{m,N_{\varphi}+1/2}=\chi_{\varphi}^{m,1/2}=0 \tag{24b}$$

$$\chi_{\theta}^{m+1/2,n}-\chi_{\theta}^{m-1/2,n}=\frac{w_{\theta}^{m}}{\sin\theta^{m}}\left\{\frac{\partial}{\partial\theta}\left[\left(\xi^{2}-1\right)\frac{\rho}{n}\frac{\partial n}{\partial\rho}-\sin^{2}\theta\cos^{2}\varphi\right]\right\}_{\Omega=\Omega^{m,n}} = -2w_{\theta}^{m}\cos\theta^{m}\left[\frac{\rho}{n}\frac{\partial n}{\partial\rho}+\cos^{2}\varphi^{n}\right] \tag{24c}$$

$$\chi_{\theta}^{N_{\theta}+1/2,n}=\chi_{\theta}^{1/2,n}=0 \tag{24d}$$

Relations between the variables with fractional indices and the variables with integer indices are needed to close the discretization. The step scheme is used to close the discretization which sets the downstream surface intensities equal to the upstream center intensities [9]. Substituting Eq. (23) into Eq. (20), the discrete ordinate form of the RTEGCN for an infinite long cylinder with axial symmetry is obtained and can be written as

$$\xi^{m,n}\frac{\partial\left(\rho I^{m,n}\right)}{\partial\rho}+\tilde{\beta}^{m,n}(\rho)I^{m,n}=\tilde{S}^{m,n}(\rho) \tag{25}$$

where $\tilde{\beta}^{m,n}$ and $\tilde{S}^{m,n}$ is defined as

$$\tilde{\beta}^{m,n}(\rho)=\frac{1}{w_\theta^m}\max\left(\chi_\theta^{m+1/2,n},0\right)+\frac{1}{w_\theta^m}\max\left(-\chi_\theta^{m-1/2,n},0\right)$$
$$+\frac{1}{w_\varphi^n}\max\left(\chi_\varphi^{m,n+1/2},0\right)+\frac{1}{w_\varphi^n}\max\left(-\chi_\varphi^{m,n-1/2},0\right) \tag{26a}$$
$$+\rho\left(\kappa_a+\kappa_s-\frac{\kappa_s}{4\pi}\Phi^{m,n;m,n}w_\theta^m w_\varphi^n\right)$$

$$\tilde{S}^{m,n}(\rho)=\rho n^2\kappa_a I_b+\rho\frac{\kappa_s}{4\pi}\sum_{m'=1,m'\neq m}^{N_\theta}\sum_{n'=1,n'\neq n}^{N_\varphi}I^{m',n'}\Phi^{m',n';m,n}w_\theta^{m'}w_\varphi^{n'}$$
$$+\frac{1}{w_\theta^m}\max\left(-\chi_\theta^{m+1/2,n},0\right)I^{m+1,n}+\frac{1}{w_\theta^m}\max\left(\chi_\theta^{m-1/2,n},0\right)I^{m-1,n} \tag{26b}$$
$$+\frac{1}{w_\varphi^n}\max\left(-\chi_\varphi^{m,n+1/2},0\right)I^{m,n+1}+\frac{1}{w_\varphi^n}\max\left(\chi_\varphi^{m,n-1/2},0\right)I^{m,n-1}$$

2.3 Finite Element Method Discretization for Single Layer

The common Galerkin scheme based finite element method for solving radiative transfer equation often suffers from nonphysical oscillation of solutions due to the convection dominated characteristics of the radiative transfer equation [14, 15] and the lower stability of the Galerkin scheme, while the least square scheme is more stable, which has been well studied for radiative transfer in uniform index medium [16] and graded index medium [9, 17]. Hence in this paper, the least square finite element method (LSFEM) is used to spatially discretize the discrete ordinate form of the RTEGCN [Eq. (25)]. The radiative intensity of direction $\mathbf{\Omega}^{m,n}$ can be approximated based on the shape functions $\phi_i(\rho)$ as

$$I^{m,n}(\rho)\simeq\sum_{i=1}^{N_{sol}}I_i^{m,n}\phi_i(\rho),\quad \rho I^{m,n}(\rho)\simeq\sum_{i=1}^{N_{sol}}\rho_i I_i^{m,n}\phi_i(\rho) \tag{27}$$

The least square finite element approach is obtained when weighted residual method is applied to equation (25) by taken the weight function as $W=\xi^{m,n}\rho_j\frac{\partial\phi_j}{\partial\rho}+\tilde{\beta}_j^{m,n}\phi_j$. For each discrete direction $\mathbf{\Omega}^{m,n}$, the final radiative transfer equation can be written in the following set of linear equations:

$$\mathbf{K}^{m,n}\mathbf{I}^{m,n}=\mathbf{H}^{m,n} \tag{28}$$

in which the stiff matrix $\mathbf{K}^{m,n}$ and the right hand side vector $\mathbf{H}^{m,n}$ are defined as

$$K_{ji}^{mn} = \xi^{m,n}\xi^{m,n}\rho_i\rho_j\int_V \frac{\partial\phi_i}{\partial\rho}\frac{\partial\phi_j}{\partial\rho}\mathrm{d}V + \xi^{m,n}\rho_j\tilde{\beta}_i^{m,n}\int_V \phi_i\frac{\partial\phi_j}{\partial\rho}\mathrm{d}V + \tilde{\beta}_j^{m,n}\xi^{m,n}\rho_i\int_V \frac{\partial\phi_i}{\partial\rho}\phi_j\,\mathrm{d}V + \tilde{\beta}_j^{m,n}\tilde{\beta}_i^{m,n}\int_V \phi_i\phi_j\,\mathrm{d}V \tag{29a}$$

$$H_j^m = \xi^{m,n}\rho_j\int_V \tilde{S}^{m,n}\frac{\partial\phi_j}{\partial\rho}\mathrm{d}V + \tilde{\beta}_j^{m,n}\int_V \tilde{S}^{m,n}\phi_j\,\mathrm{d}V \tag{29b}$$

As seen from Eq. (29), the least square finite element discretization leads to a symmetric stiff matrix for every discrete ordinate direction, which is a very good numerical property.

2.4 Relationship of Radiative Intensity between Two Adjacent Layers

The solution of radiative transfer in a single layer cylindrical medium has been well defined in previous sections. In this and the following sections, issues on the extension of the method to deal with multilayer cylindrical medium will be discussed.

According to the Snell's law and energy conservation, when a ray travels from first layer to the second layer (as shown in Fig. 2), the following relation holds for the radiative intensities at the interface [18]:

$$(1-\rho_{f,1\to2})\frac{I_1}{n_1^2} = \frac{I_2}{n_2^2} \tag{30}$$

where I_1 and I_2 are the incident radiative intensity at the left side and the transmitted intensity at the right side of the interface, respectively; $\rho_{f,1\to2}$ denotes the Fresnel reflectivity when the ray travels from the first layer to the second layer. Without considering polarization, $\rho_{f,1\to2}$ can be expressed as

$$\rho_{f,1\to2} = \frac{1}{2}\left(R_S + R_P\right) \tag{31}$$

where

$$R_S = \left|r_S\right|^2, \quad R_P = \left|r_P\right|^2 \tag{32}$$

$$r_S = \frac{\cos\theta_i - \sqrt{m^2+\cos^2\theta_i - 1}}{\cos\theta_i + \sqrt{m^2+\cos^2\theta_i - 1}}, \quad r_P = \frac{m^2\cos\theta_i - \sqrt{m^2+\cos^2\theta_i - 1}}{m^2\cos\theta_i + \sqrt{m^2+\cos^2\theta_i - 1}} \tag{33}$$

where θ_i is the incident angle, $m = n_2/n_1$ is the relative refractive index; R_S and R_P are the reflectivity of S polarization and P polarization, respectively; r_S and r_P are the amplitude reflection coefficients of S

polarization and P polarization, respectively.

Because the direction of incidence changes after refraction, the refracted direction often does not belong to the discrete ordinates set. This is a problem for the discrete ordinates solution on each layer. The problem can be solved by an angular interpolation approach to obtain the intensity of directions that belongs to the discrete ordinates set (depicted in Fig. 2).

2.5 Angular Interpolation of Interface Intensity between Two Adjacent Layers

With the help of the new cylindrical coordinate system, the interpolation in the two dimensional angular space is reduced to a one-dimensional interpolation problem in the optical plane, which will be discussed below. The relationship of reflection and refraction at the cylindrical interface between two adjacent layers is shown in Fig. 3. It can be seen that optical plane of reflection and refraction is defined by the azimuthal angle φ_i correspond to the incident direction $\mathbf{\Omega}''$. As such, the interpolation of intensity of the refracted direction $\mathbf{\Omega}'''$ in the whole solid angular space can be conducted only over the plane determined by φ_i, namely, only one-dimensional interpolation over the optical plane is needed. The argument of the interpolation function is the local zenith angle θ. This is the same as the case of one-dimensional infinite parallel plates.

The radial basis function is used here to conduct the angular space interpolation. It has many advantages to use radial basis function to do interpolation, such as the interpolation nodes can be arbitrarily scattered, being easily to program, high accuracy of interpolation can be obtained, and easily to be extended to higher dimensional problems, etc. Currently, the radial basis function has been widely applied to the interpolation of scattered data [19, 20] and used in meshless method to solve partial differential equations [20, 21]. Some commonly used radial basis functions [20] are presented in Table 1, in which the first three are the global radial basis functions, while the others are the compactly supported radial basis functions.

The procedure of interpolation using radial basis functions is given following. Firstly, the intensity is approximated by the radial basis function in the meridian plane of φ_i as

$$I_{\varphi_i}(\theta) \approx \sum_{j=1}^{N_\theta} \alpha_l \Re\left(\left|\theta_l - \theta\right|\right) \tag{34}$$

The constraint of interpolation requires

$$I_{\varphi_i}(\theta_m) = \sum_{m=1}^{N_\theta} \alpha_l \Re\left(\left|\theta_l - \theta_m\right|\right) \tag{35}$$

As such, a system of linear equations about the expansion coefficient α_l can be obtained, which is written in matrix form as

$$\mathbf{\Phi}\,\boldsymbol{\alpha} = \mathbf{u} \tag{36}$$

where $\mathbf{\Phi} = \left[\Phi_{lm}\right]_{N_\theta \times N_\theta} = \left[\Re(\left|\theta_l - \theta_m\right|)\right]_{N_\theta \times N_\theta}$, $\boldsymbol{\alpha} = \left[\alpha_l\right]_{l=1,N_\theta}$ and $\mathbf{u} = \left[I_{\varphi_i}(\theta_m)\right]_{m=1,N_\theta}$. Hence the expansion coefficient is obtained as $\boldsymbol{\alpha} = \mathbf{\Phi}^{-1}\mathbf{u}$.

Generally, there are two schemes to interpolate the radiative intensity between the interface of two adjacent layers, (1) forward interpolation, this is based on the forward ray tracing, and all the refracted directions are selected as the interpolation nodes; (2) backward interpolation, this is based on the back forward ray tracing. The incident direction is inversely obtained through the refracted direction based on Fresnel's law, and all the directions before refraction are selected as interpolation nodes. Our numerical experiments reveal that the first scheme is less stable than the second scheme. This may be due to the refracted directions varying with different refractive indices of the adjacent layers, and which will result in some kind of randomization. However, the second scheme does not have this problem, for the interpolation nodes is always selected as the incident directions. As such, the second angular interpolation is used in following section.

In order to make a comparison of the performance of different radial basis functions in angular interpolation, angular intensity interpolation between two homogeneous layers is considered. The refractive indices of the left and right layers are $n_L = 1$ and $n_R = 2.5$, respectively. Because $n_L < n_R$, the radiative energy will converge for the reason of refraction in case the incidence is from left side. For the incidence from right side, total reflection will happen in some angular region.

The incidence from the left side of the interface with an intensity I_0 is considered, and the radial basis function is used to interpolate the refracted intensity distribution transmit the left layer into the right layer. Figure 4 (a) and 4(b) present the interpolated intensity obtained by several different radial basis functions, and which are compared to the exact results under angular discretization of N_θ=30 and N_θ=100, respectively. Here, the support domain of the Wendland type radial basis functions are all taken as $0.2\max(w_\theta)$. It is seen that the accuracy of interpolation by compactly supported radial basis function depend much on the size of support domain. If the size of support domain is not selected appropriately, the interpolated result will not be stable even the angular discretization is refined. As compared to the compactly supported radial basis functions, additional adjustment parameter is not required for the global radial basis function and stable interpolation results are obtained under different refinement of angular grid. By comparison, the global radial basis function IMQ is selected in the following section to do angular interpolation.

2.6 Treatment of Multilayer Fresnel Boundary and Implementation

The basic idea for solving radiative transfer in multilayer cylindrical medium is that each layer is treated as medium with continuous refractive index distribution and solved separately. The key problem is how to couple the radiative intensity between adjacent layers. In this section, the coupled relation of radiative intensity between adjacent layers is discussed and the detailed solution procedure for solving radiative transfer in multilayer cylindrical medium is described. In order to solve radiative transfer in each layer separately, boundary condition is needed for each layer, which can be obtained from the coupled relation of intensity at the interface. The configuration of a radial multilayer medium is shown in Fig. 5. For the *i*th layer, the radiative intensity at the interface is composed of the transmitted intensity from adjacent layer and the reflected intensity originates from the same layer. Because the optical plane is the isometric plane of local azimuthal angle φ, the boundary condition at the interface can be written shortly as

$$I_{i,L}(\theta)=\left[1-\rho_{f,i-1\to i}(\cos\tilde{\theta})\right]\frac{n_i^{\,2}}{n_{i-1}^{\,2}}I_{i-1,R}(\tilde{\theta})+\rho_{f,i\to i-1}(\cos\theta'')I_{i,L}(\theta''),\ \ \cos\theta>0 \tag{37a}$$

$$I_{i,R}(\theta)=\left[1-\rho_{f,i+1\to i}(\cos\tilde{\theta})\right]\frac{n_i^{\,2}}{n_{i+1}^{\,2}}I_{i+1,L}(\tilde{\theta})+\rho_{f,i\to i+1}(\cos\theta'')I_{i,R}(\theta''),\ \ \cos\theta<0 \tag{37b}$$

where $I_{i,L}(\theta)$ and $I_{i,R}(\theta)$ denote the radiative intensity of local zenith angle θ at the left and the right boundary of the *i*th layer, respectively; $\rho_{f,i-1\to i}$ is the Fresnel reflection coefficient for incident radiation from the (*i*-1)th layer to the *i*th layer [obtained by Eq. (31)], which is a function of incident angle and relative refractive index of the adjacent layer; $\tilde{\theta}$ is the corresponding coming incident direction of the refracted direction θ; θ'' is the corresponding coming incident direction of the reflection direction θ. The first term of the right hand side of Eq. (37) accounts for the contribution of transmitted energy from adjacent layer, and the second term accounts for the contribution of reflected energy from internal reflection of the same layer.

To ensure convergence of layer by layer solution, upwinding treatment is needed to impose boundary condition for each layer only on the upwind boundary. The implementation of solving the radiative transfer equation in multilayer cylinder can be carried out according to the following routine:

1） Begin angular loop and determine the optical plane. For discrete direction $\mathbf{\Omega}^{m,n}=(\theta^m,\varphi^m)$, the optical plane is determined as $\varphi=\varphi^n$.

2） Solve the radiative intensity distribution in the 1st layer. Firstly, calculate the stiff matrix related to the first layer based on Eq. (29). Then the boundary condition is imposed on the upwind boundary by checking the sign of $\cos\theta^m$ (if $\cos\theta^m$ >0 the upwind boundary is the left boundary, and if $\cos\theta^m$ <0 the upwind boundary is the right boundary). If the determined boundary is a interface between two adjacent layers, the intensity at this interface is computed by Eq. (37), where the transmitted radiative intensity is obtained by angular interpolation by radial basis functions. The corresponding coming incident direction of reflection of direction $\mathbf{\Omega}^{m,n}$ is $\mathbf{\Omega}^{N_\theta-m+1,n}$.

3） Calculate the radiative intensity distribution of the 2nd layer. The solution procedure, imposing of boundary

condition, and treatment of interface between adjacent layers are the same as the 1st layer.

4） If the multilayer medium composed of *n* layer, loop each layer, and solve the radiative intensity distribution following the approach of the 1st layer described above.

3 RESULTS AND DISCUSSION

Based on the formulation described above, a computer code capable of modeling radiative transfer problems in an infinitely long multilayer cylindrical graded index medium has been developed. Three various test cases are selected to verify the performance of the finite element method. The absorption and the scattering coefficients of the medium enclosed by the enclosure are uniform. For the sake of comparison, the relative error based on data in the references is defined as

$$\text{Relative Error }\% = \frac{\int \left|\text{FEM solution }(r) - \text{Benchmark result }(r)\right| dr}{\int \left|\text{Benchmark result }(r)\right| dr} \times 100 \tag{38}$$

3.1 Case 1: Semitransparent Cylinder with Fresnel Boundary

A semitransparent uniform index cylindrical medium with Fresnel boundary is considered. The temperature of surroundings is $T_0 = 1000\text{K}$, while the cylindrical medium is nonscattering and nonemitting. The LSFEM is applied to this case with 40 isoparametric linear elements and the total solid angle is subdivided as $N_\theta \times N_\varphi = 200 \times 200$. Figure 6(a) and 6(b) present the dimensionless radial distributions of volumetric radiative absorption and dimensionless incident radiation, respectively, for three different optical thickness, namely $\tau_R = \kappa_a R = 1.0$, 5 and 10, and the refractive index $n = 1.2$, which are also compared with the results obtained using ray tracing method [22]. The dimensionless volumetric absorption α_V follows the same definition given in Ref. [22],

$$\alpha_V(\rho) = \frac{\mathrm{d}q_\rho}{\mathrm{d}\rho}\frac{\pi R^2}{2q_\rho(R)\pi R} = \frac{\mathrm{d}q_\rho}{\mathrm{d}\rho}\frac{R}{2q_\rho(R)} \tag{39}$$

As seen from Fig. 6, the results obtained using LSFEM are in good agreement with the results obtained using ray tracing method [22], the maximum relative error based on the data of ray tracing method is less than 2.5%.

3.2 Case 2: Parabolic Refractive Index Distribution with Fresnel Boundary inside Cylindrical Medium

We consider radiative transfer problem in a graded index one-dimensional nonscattering semitransparent cylinder with Fresnel boundary. The temperature of the surroundings and the cylindrical medium are $T_0 = 1000\text{K}$ and $T_g = 0\text{K}$, respectively. The refractive index within the cylinder varies parabolically with the radius as $n(\rho) = \sqrt{4-(\rho/R)^2}$. For this distribution of refractive index, the ray trajectory can be obtained analytically [23], hence a ray tracing method following Liu [24] is convenient to be developed to obtain the intensity distribution. The LSFEM is applied to this case with 40 isoparametric linear elements and the total solid angle is subdivided as $N_\theta \times N_\varphi = 200 \times 200$. Figure 7(a) and 7(b) present the solved radial dimensionless net radiative heat flux distributions and dimensionless incident radiation along the radial coordinate, respectively, for three different values of absorption coefficient, namely, $\tau_R = \kappa_a R = 1.0$, 5, and 10, which are compared with the solutions obtained by ray tracing method as benchmark. It can be seen that the results obtained using the LSFEM are in good agreement with the benchmark results for different values of absorption coefficient. The maximum relative error based on the data of benchmark results is less than 2.3%.

3.3 Case 3: Infinite Long Hollow Cylinder with Fresnel Boundary

The dimensionless incident radiation of an infinitely long hollow cylinder with Fresnel surfaces is calculated numerically using the LSFEM. Figure 8 compares the distribution of the dimensionless incident radiation obtained by the LSFEM with the results obtained using ray tracing method [25] for three cases: $\tau_{R_O} = 1$, $\tau_{R_i}/\tau_{R_o} = 0.5$, $n = 1.5$; $\tau_{R_o} = 1$, $\tau_{R_i}/\tau_{R_o} = 0.1$, $n = 1.5$ and $n = 2$. The temperature of surroundings and cylindrical medium are $T_o = 1000\text{K}$ and $T_g = 0\text{K}$, respectively. The cylindrical medium is non scattering and emitting. Both spatial and angular discretizations are refined to ensure convergence of final results. The LSFEM is applied to this case with 10 isoparametric linear elements on each layer and the total solid angle is subdivided as

$N_\theta \times N_\varphi = 200 \times 200$. It can be seen that the results obtained using the LSFEM are in good agreement with the benchmark results in reference. The maximum relative error based on the data of ray tracing method is less than 1%.

As seen from Fig. 8, the dimensionless incident radiation near the inner surface is higher than the incident radiation near the outer surface for both $\tau_{R_i} / \tau_{R_o} = 0.5$ and $\tau_{R_i} / \tau_{R_o} = 0.1$, which is due to the rays being refracted toward the center at the outer surface, hence much energy are concentrated near the inside surface. The dimensionless incident radiation has distinctive difference when the refractive index varies from $n = 1.5$ to $n = 2$. The effects of a Fresnel surface on incident radiation are more prominent with large refractive index because of the increased refraction.

3.4 Case 4: Two-Layer Graded Index Cylindrical Medium

Three test problems of two-layer cylindrical medium with different variable refractive index distributions bounded by Fresnel wall are considered in this case. Detailed definition of the three problems is given in Table 2. The first problem is a simple case in which the inner layer is vacuum, while the outer layer is a cold absorbing medium. In the second problem, both the inner layer and the outer layer are cold absorbing medium and have graded index distributions. Scattering is involved in the third case, in which the inner layer is isotropically scattering and absorbing and has a parabolic type refractive index distribution as studied in Case 2, while the outer layer is nonscattering with a uniform refractive index distribution. In all three test problems, the temperature and refractive index of the surrounding medium are taken as $T_o = 1000\text{K}$ and $n = 1$.

Figure 9(a) and 9(b) present the solved radial dimensionless net radiative heat flux distributions and the dimensionless incident radiation along the radial coordinate, respectively, for test problem 1 by the LSFEM. The refractive index distribution in the outer layer is $n(\rho) = k\rho / R + 2$, in which the slope parameter is taken as k=0.1, 1, 1.5 and 2 respectively. The LSFEM is applied to this problem with 10 isoparametric linear elements in the inner layer, 20 isoparametric linear elements in the outer layer along the radial direction, and the total solid

angle is subdivided as $N_\theta \times N_\varphi = 200 \times 200$. It is observed that the heat flux penetrating into the medium decreases with increasing the gradient of outer layer index distribution. At the same time, an inflection point exists in the radial distribution of heat flux due to the discontinuity of refractive index at the interface between the two layers. The incident radiation distribution also decreases with increasing the gradient of outer layer index distribution. As the incident radiation is a measure of volume absorption for external irradiation, it indicates that the volume absorption decreases with the increasing of the gradient of refractive index distribution inside the outer layer. This conforms to the decrease of total heat flux penetrating into the medium. A discontinuity is observed in the radial distribution of incident radiation, which is due to the discontinuity of refractive index distribution at the interface. The refractive index distribution of the outer layer significantly influences radiative absorption in the multilayer cylindrical medium.

Figure 10(a) and 10(b) present the solved radial dimensionless net radiative heat flux distributions and the dimensionless incident radiation along the radial coordinate, respectively, for test problem 2. The LSFEM is applied to this case with 20 isoparametric linear elements in the inner and outer layer along the radius direction, respectively, and the total solid angle is subdivided as $N_\theta \times N_\varphi = 200 \times 200$. The heat flux penetrating into the medium decreases with the increasing of the gradient of refractive index distribution inside the outer layer, which conforms to the trend of the incident radiation distribution. This observation is similar to the case that the inner layer has a uniform index distribution [Fig. 9(a)]. However, the trends of distribution of radiative heat flux and incident radiation vary substantially when the refractive index distribution inside the inner layer has a parabolic profile, which is due to the curved ray trajectory induced by the graded index distribution.

Figure 11(a) and 11(b) present the solved radial dimensionless net radiative heat flux distributions and the dimensionless incident radiation along the radial coordinate, respectively, for test problem 3. The LSFEM is applied to this case with 10 isoparametric linear elements in the inner and outer layer, respectively, and the total solid angle is subdivided as $N_\theta \times N_\varphi = 200 \times 200$. It is observed that the dimensionless heat flux penetrating

into the medium hold a value about 0.6 for different scattering albedo, which indicates the total absorption of the two-layer medium are affected little by scattering process. However, the trends of radial distribution of internal radiative heat flux and the incident radiation are substantially altered with different strength of scattering. For a bigger scattering albedo, more incident radiation is scattered, as such, the incident radiation is smaller at the center of cylindrical medium.

4 CONCLUSIONS

A new radiative transfer equation is derived based on a new cylindrical coordinate system in order to deal with the specular reflection and the Fresnel boundary. A Least squares finite element method is developed for solving the radiative transfer equation for graded index medium in the new cylindrical coordinate system. For multi-layer cylindrical medium, a radial basis function interpolation method is proposed to couple the radiative intensity at the interface between two adjacent layers. Various problems of both solid cylinder and multilayer cylinder and with medium of uniform refractive index distribution and graded refractive index distribution are tested. The results show that the finite element approach presented in this paper has good accuracy in predicting radiative transfer in semitransparent graded index cylindrical medium with Fresnel boundary, and the presented method can also solve radiative transfer in multilayer cylindrical medium precisely.

ACKNOWLEDGEMENT

The support of this work by the National Nature Science Foundation of China (50620120442, 50836002) is gratefully acknowledged.

REFERENCES

[1] Ben Abdallah P and Le Dez V. Thermal emission of a semi-transparent slab with variable spatial refractive index. JQSRT 2000; 67: 185-98.

[2] Ben Abdallah P, Charette A and Le Dez V. Influence of a spatial variation of the thermo-optical

constants on the radiative transfer inside an absorbing–emitting semi-transparent sphere. JQSRT 2001; 70: 341-65.

[3] Xia XL, Huang Y and Tan HP. Thermal emission and volumetric absorption of a graded index semitransparent medium layer. JQSRT 2002; 74: 235-48.

[4] Huang Y, Xia XL and Tan HP. Temperature field of radiative equilibrium in a semitransparent slab with a linear refractive index and gray walls. JQSRT 2002; 74: 249-61.

[5] Huang Y, Dong SJ, Yang M and Wang J. Thermal emission characteristics of a graded index semitransparent medium. JQSRT 2008; 109: 2141-50.

[6] Ben Abdallah P, Fumeron S, Le Dez V and Charette A. Integral form of the radiative transfer equation inside refractive cylindrical media. J Thermophys Heat Transfer 2001; 15: 184-9.

[7] Liu LH, Zhang L and Tan HP. Radiative transfer equation for graded index medium in cylindrical and spherical coordinate systems. JQSRT 2006; 97: 446-56.

[8] Modest MF. Radiative heat transfer. 2nd ed. New York: Academic Press; 2003.

[9] Zhang L, Zhao JM and Liu LH. Finite element method for modeling radiative transfer in semitransparent graded index cylindrical medium. JQSRT 2009; 110: 1085-96.

[10] Wei Z, Lee K, Tchikanda SW and Zhou Z. Effects of radiative transfer modeling on transient temperature distribution in semitransparent glass rod. Journal of Heat Transfer 2003; 125: 635-43.

[11] Yin Z and Jaluria Y. Thermal transport and flow in high-speed optical fiber drawing. Journal of Heat Transfer 1998; 120: 916-30.

[12] Lemonnier D and Le Dez V. Discrete ordinates solution of radiative transfer across a slab with variable refractive index. JQSRT 2002; 73: 195-204.

[13] Liu LH, Zhang L and Tan HP. Finite element method for radiation heat transfer in multi-dimensional graded index medium. JQSRT 2006; 97: 436-45.

[14] Chai JC, Lee HS and Patankar SV. Finite-volume method for radiation heat transfer. In: Minkowycz WJ and Sparrow EM, editors. Advances in numerical heat transfer, vol. 2. New York: Taylor & Francis; 2000. p. 109-41.

[15] Zhao JM and Liu LH. Second order radiative transfer equation and its properties of numerical solution using finite element method. Numer Heat Transfer B 2007; 51: 391-409.

[16] Zhao JM and Liu LH. Spectral element method with adaptive artificial diffusion for solving radiative transfer equation. Numer Heat Transfer B 2008; 53 536-54.

[17] Liu LH. Least-squares finite element method for radiation heat transfer in graded index medium. JQSRT 2007; 103: 536-44.

[18] Siegel R and Howell JR. Thermal radiation heat transfer. fourth ed. New York: Taylor and Francis; 2002.

[19] Narcowich FJ. Recent developments in error estimates for scattered-data interpolation via radial basis functions. Numerical Algorithms 2007; 39: 307-15.

[20] Wu ZM and Schaback R. Local error estimates for radial basis function interpolation of scattered data. IMA Journal of Numerical Analysis 1993; 13: 13-27.

[21] Flyer N and Wright GB. Transport schemes on a sphere using radial basis functions. J Comput Phys 2007; 226: 1059-84.

[22] Liu LH, Tan HP and Yu QZ. Internal distribution of radiation absorption in one-dimensional semitransparent medium. International Journal of Heat and Mass Transfer 2002; 45: 417-24.

[23] Marchand EW. Ray tracing in cylindrical gradient-index media. Appl Opt 1972; 11: 1104-6.

[24] Liu LH. Discrete curved ray-tracing method for radiative transfer in an absorbing-emitting semitransparent slab with variable spatial refractive index. JQSRT 2004; 83: 223-8.

[25] Tian WX and Chiu WKS. Radiative absorption in an infinitely long hollow cylinder with Fresnel

surfaces. JQSRT 2006; 98: 249-63.

Table 1. Commonly used radial basis functions

RBF	$\Re(r)$
MQ	$\left(1+r^2\right)^{\frac{1}{2}}$
IMQ	$\left(1+r^2\right)^{-\frac{1}{2}}$
G	$\exp\left(-r^2\right)$
Wendland C^0	$\left(1-r^2\right)_+^2$
Wendland C^2	$\left(1-r^2\right)_+^4\left(4r+1\right)$
Wendland C^4	$\left(1-r^2\right)_+^6\left(35r^2+18r+3\right)$

Table 2. Physical definitions of problems studied in Case 4.

Problem	Layer 1 (inner layer)	Layer 2 (outer layer)	Surrounding
1	vacuum	cold and nonscattering; $\tau_{R_o} = \kappa_a R_o = 1$; $n(\rho) = k\rho / R + 2$; k=0.1, 1, 1.5 and 2.	$T_0 = 1000\text{K}$ $n = 1$
2	cold and nonscattering; $\tau_{R_i} = \kappa_a R_i = 0.5$; $n(\rho) = \sqrt{4 - (\rho / R)^2}$.	cold and nonscattering; $\tau_{R_o} = \kappa_a R_o = 1$; $n(\rho) = k\rho / R + 2$; k=0.1, 1 and 2.	$T_0 = 1000\text{K}$ $n = 1$
3	cold and isotropic scattering, $\omega = 0.1$, 0.5, and 0.9; $\tau_{R_i} = \kappa_a R_i = 0.5$; $n(\rho) = \sqrt{4 - (\rho / R)^2}$.	cold and nonscattering; $\tau_{R_o} = \kappa_a R_o = 1$; $n(\rho) = 4$.	$T_0 = 1000\text{K}$ $n = 1$

FIGURE CAPTIONS

Figure 1. Definition of variables in cylindrical coordinate systems: (a) traditional cylindrical coordinate system (b) new cylindrical coordinate system.

Figure 2. Refraction relationship between two adjacent layers.

Figure 3. The schematic of reflection and refraction between layers.

Figure 4. Interpolated angular distribution of intensity at the right side of the interface subjected to incident irradiation from left side of the interface, **(a)** $N_\theta = 30$ and **(b)** $N_\theta = 100$.

Figure 5. Configuration of radial multilayer medium.

Figure 6. Radial distributions of volumetric radiative absorption and dimensionless net radiative heat flux: **(a)** volumetric radiative absorption **(b)** dimensionless net radiative heat flux.

Figure 7. Radial distributions of dimensionless net radiative heat flux and incident radiation in the cylindrical medium with parabolic refractive index distribution: **(a)** radiative heat flux **(b)** incident radiation.

Figure 8. Dimensionless radial incident radiation distribution in the infinite long hollow cylinder.

Figure 9. Radial distributions of dimensionless net radiative heat flux and incident radiation for the problem 1 of Case 4: **(a)** radiative heat flux **(b)** incident radiation.

Figure 10. Radial distributions of dimensionless net radiative heat flux and incident radiation for the problem 2 of Case 4: **(a)** radiative heat flux **(b)** incident radiation.

Figure 11. Radial distributions of dimensionless net radiative heat flux and incident radiation for the problem 3 of Case 4: **(a)** radiative heat flux **(b)** incident radiation.

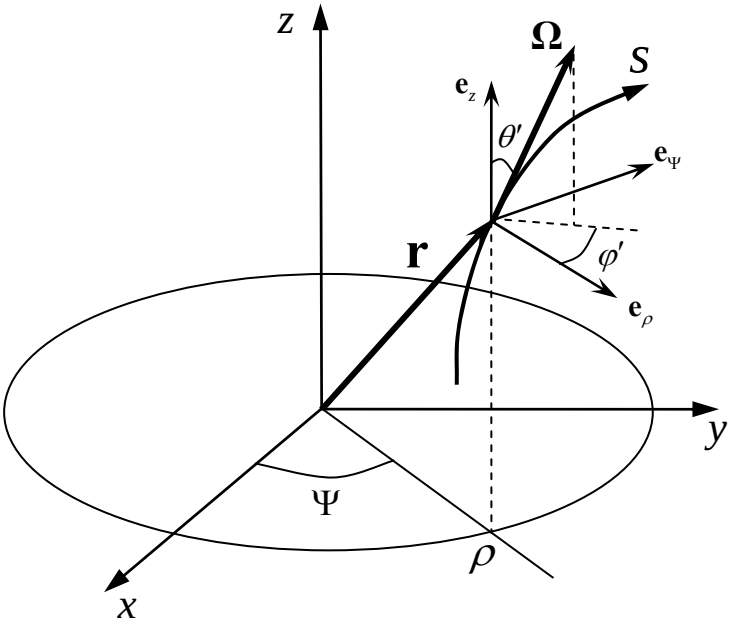

Figure 1(a)

Authors: Zhang, Zhao and Liu

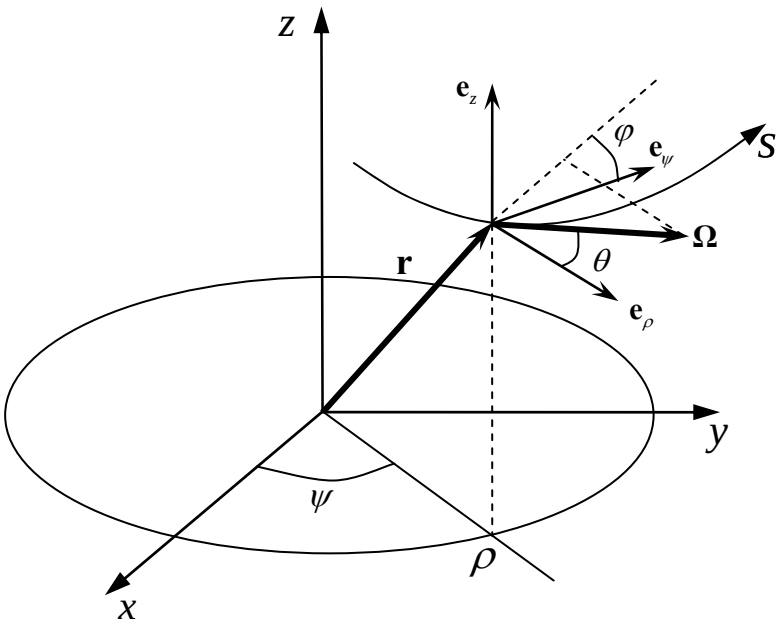

Figure 1(b)

Authors: Zhang, Zhao and Liu

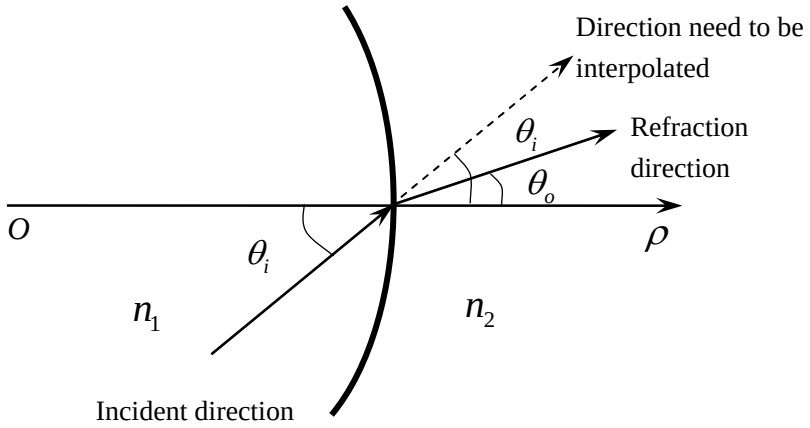

Figure 2

Authors: Zhang, Zhao and Liu

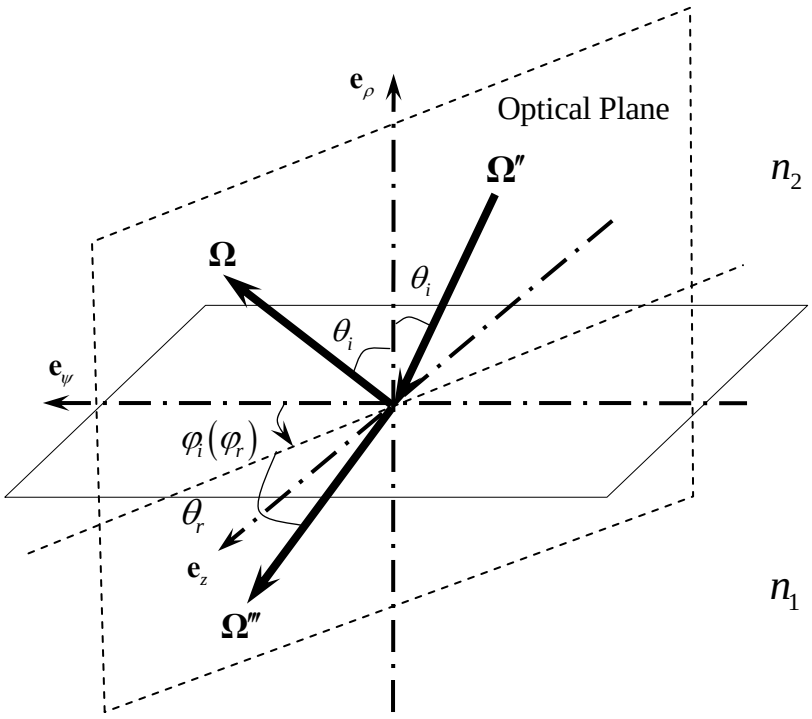

Figure 3

Authors: Zhang, Zhao and Liu

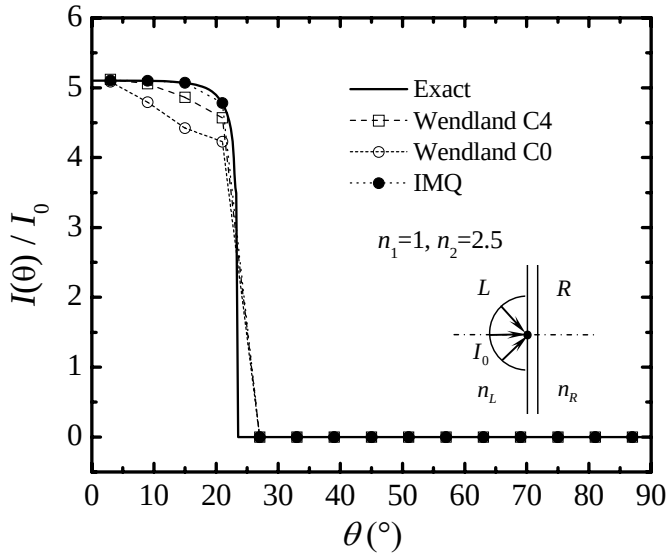

Figure 4 (a)

Authors: Zhang, Zhao and Liu

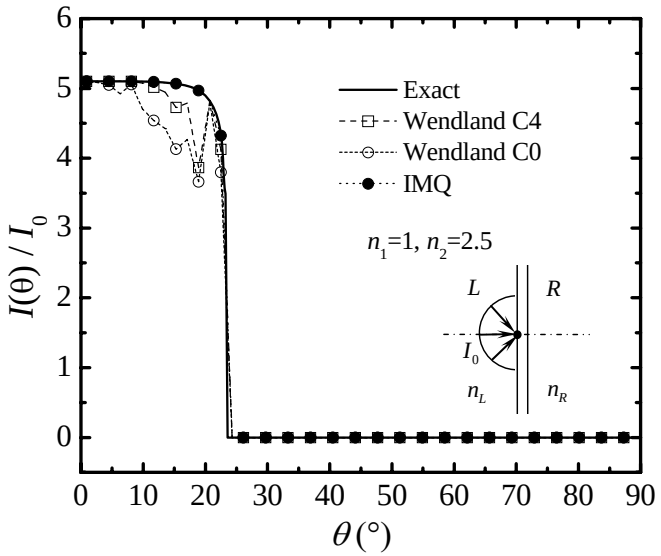

Figure 4 (b)

Authors: Zhang, Zhao and Liu

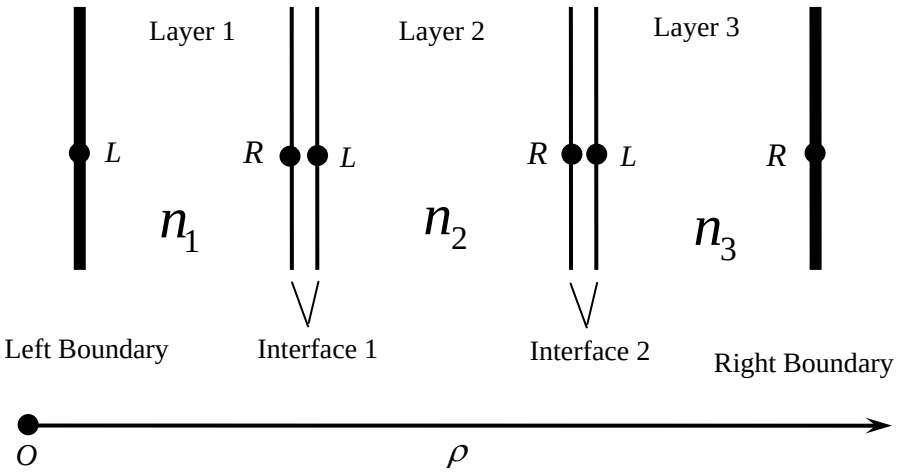

Figure 5

Authors: Zhang, Zhao and Liu

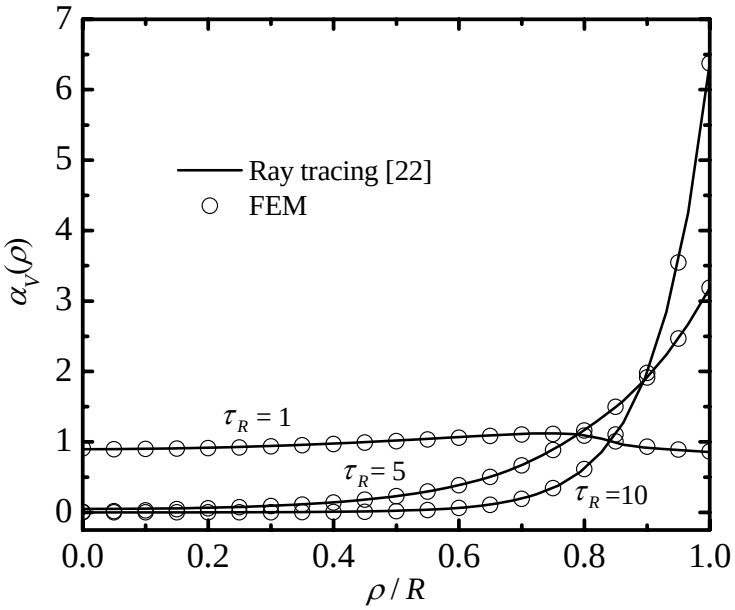

Figure 6(a)

Authors: Zhang, Zhao and Liu

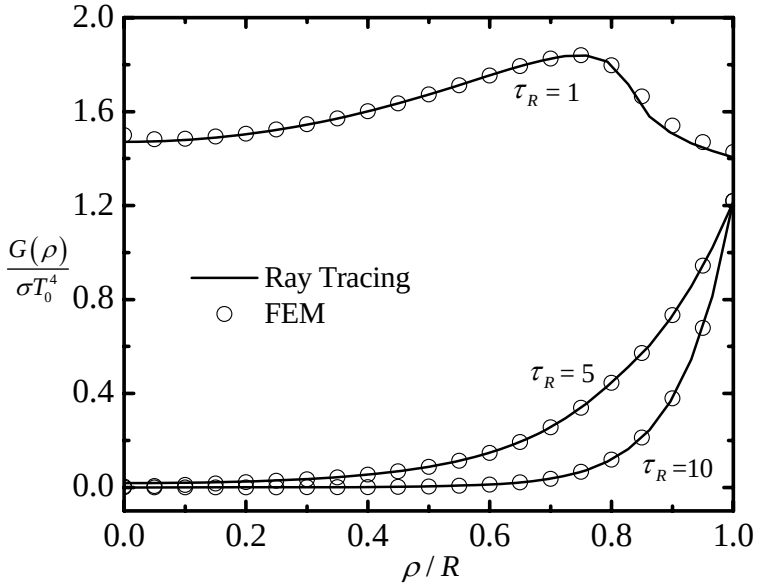

Figure 6(b)

Authors: Zhang, Zhao and Liu

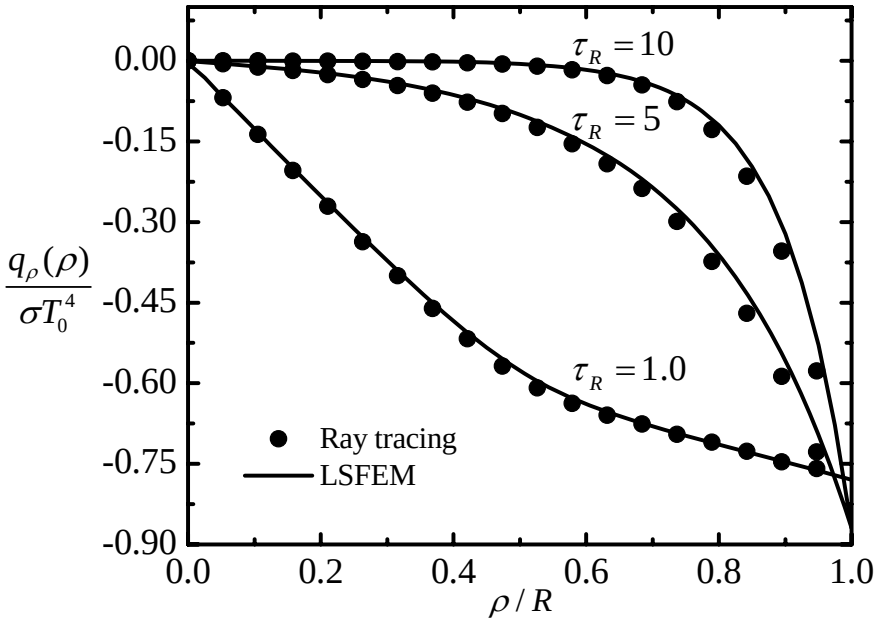

Figure 7(a)

Authors: Zhang, Zhao and Liu

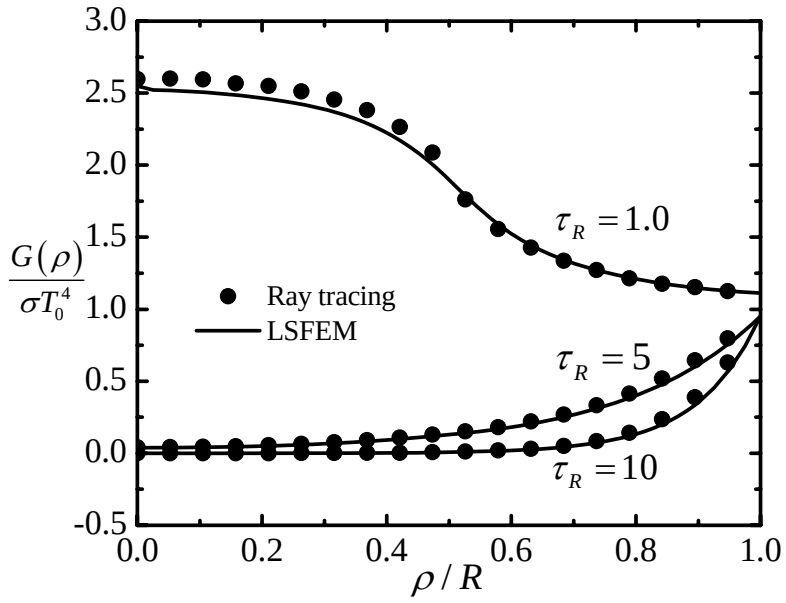

Figure 7(b)

Authors: Zhang, Zhao and Liu

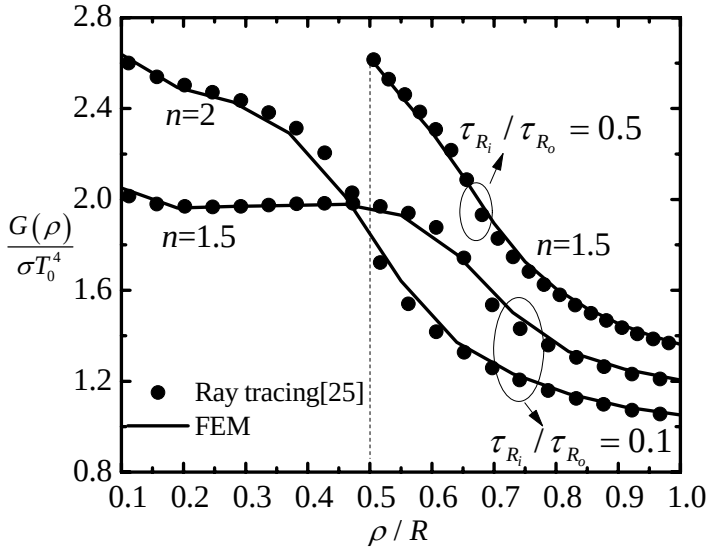

Figure 8

Authors: Zhang, Zhao and Liu

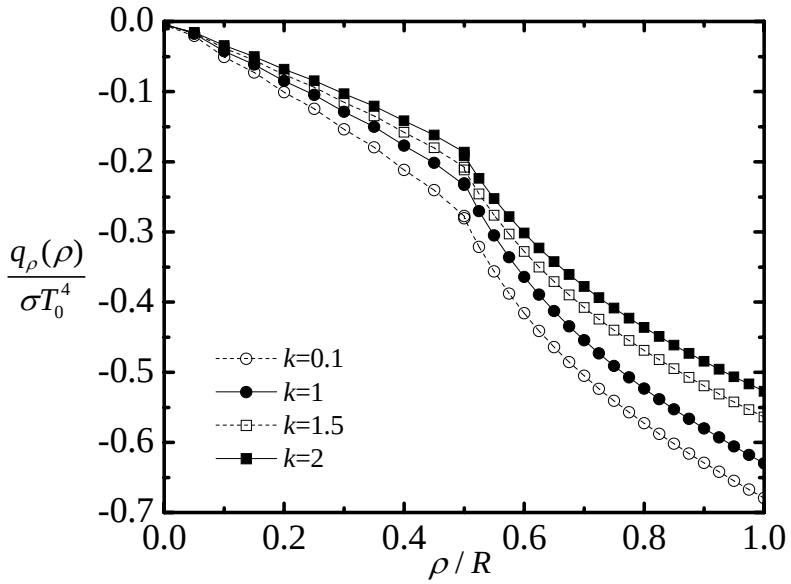

Figure 9(a)

Authors: Zhang, Zhao and Liu

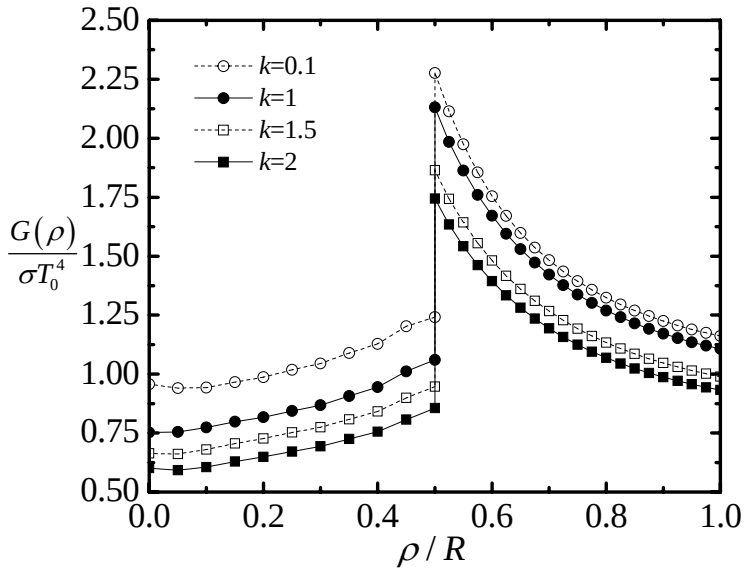

Figure 9(b)

Authors: Zhang, Zhao and Liu

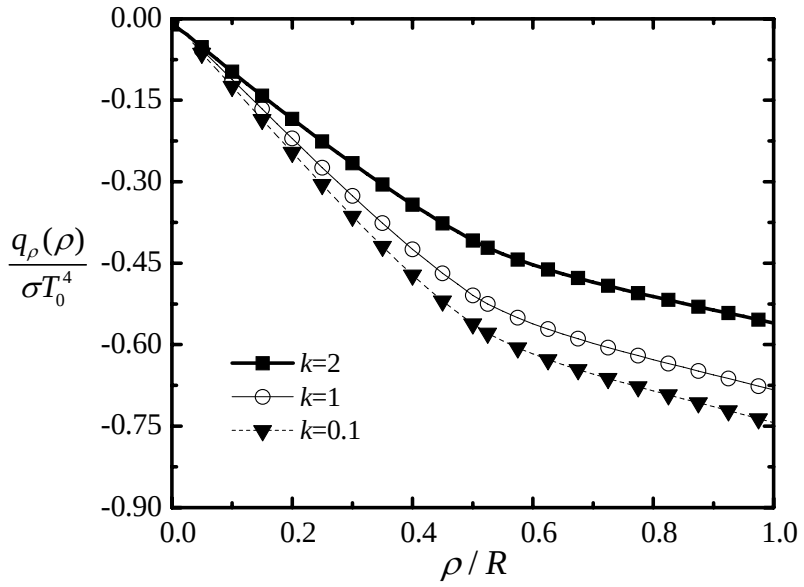

Figure 10(a)

Authors: Zhang, Zhao and Liu

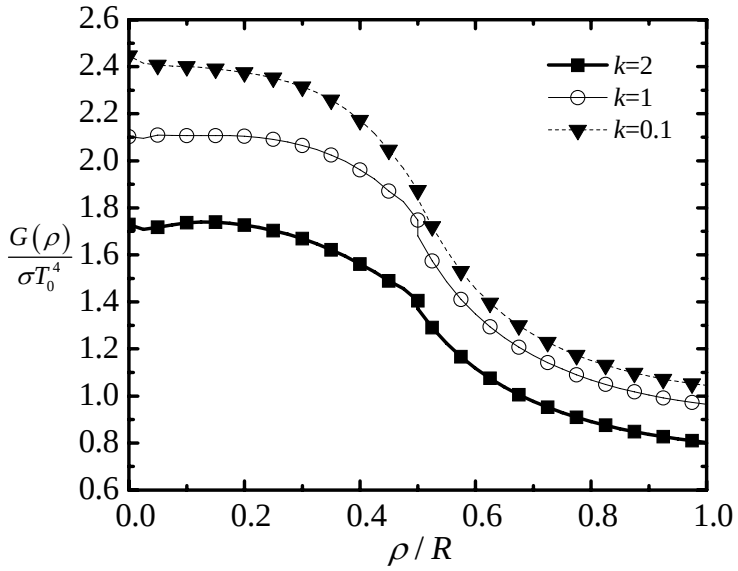

Figure 10(b)

Authors: Zhang, Zhao and Liu

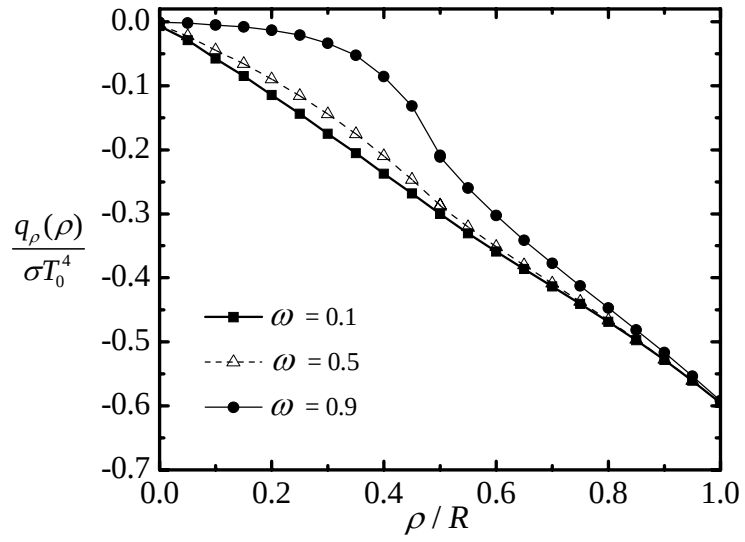

Figure 11(a)

Authors: Zhang, Zhao and Liu

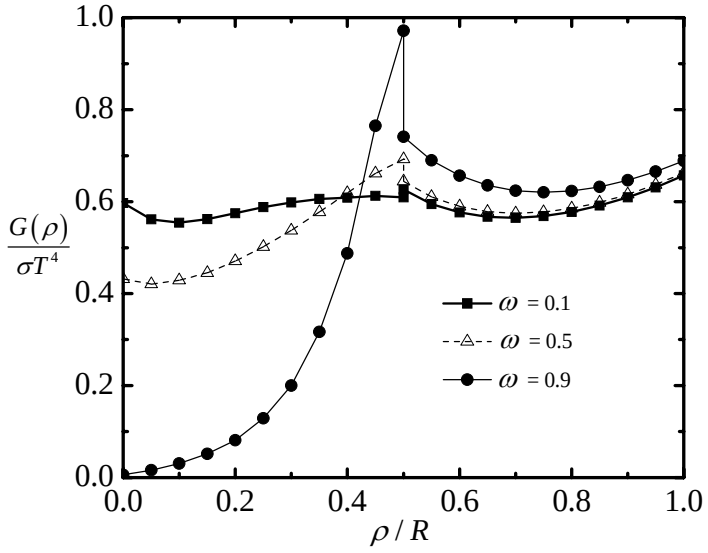

Figure 11(b)

Authors: Zhang, Zhao and Liu